LOX/Propane and LOX/Ethanol Combustion Chamber Heat Transfer

Leonard Schoenman*
Aerojet TechSystems, Sacramento, California 95813

The gas-side heat transfer rates for LOX/propane and LOX/ethanol are experimentally characterized using a 1000-lb-thrust water-cooled calorimeter chamber operating at a chamber pressure of 300 psia[2]. The effect of injector element type and fuel film cooling is defined as a function of mixture ratio. The interaction of fuel injected through the resonator cavities on heat transfer and wall soot buildup are displayed as a function of time, axial distance, fuel coolant flow rate, and mixture ratio. Comparisons between clean-burning ethanol and sooting propane show a large difference between the two fuels and significantly higher-than-expected heat-flux levels for ethanol in the throat region.

Nomenclature

C_{g_f} = coefficient in convective heat transfer equation based on frozen chemistry
C_{g_s} = coefficient in convective heat transfer equation based on equilibrium chemistry, C_g frozen/(C_{p_s}/C_{p_f})
C_{p_f} = gas heat capacity frozen properties, evaluated at T_f, Btu/lbm-°R
C_{p_s} = $\Delta H/\Delta T = H_c - H_w/T_c - T_{w_g}$
D = diameter, in.
H_c, H_w = enthalpy of gas at combustion temperature and wall temperature at local pressure
I_{sp} = specific impulse, lbf-s/lbm
$O/F, MR$ = oxidizer-to-fuel mass flow ratio
Pr_f = gas Prandtl number, evaluated at T_f, °R
Q/A = gas-side heat flux, Btu/s-in.^{2}
T_e = freestream combustion gas temperature, °R
T_f = (film temperature = $T_r + T_{w_g})/2$, °R
T_r = $T_e + Pr_f^{1/3}(T_c - T_e)$
T_{w_g} = gas-side wall temperature, °R
V = velocity, ft/s
$\dot{w}_t$ = total propellant flow rate, lbm/s
α_1 = divergence angle of LOX jet in OFO element
α_2 = divergence angle of fuel jet in OFO element
ϵ = nozzle expansion ratio
η = energy release efficient, %
θ = jet impingement half-angle
μ_f = gas viscosity, evaluated at T_f, ° lbm/in.-s
ρ = density, lb/ft^3

Introduction

THE next generation of liquid propellant rocket booster engines will most likely employ liquid oxygen (LOX) and a hydrocarbon fuel and operate at combustion pressures 50–100% greater than past designs characterized by the F-1 engine, which operated at 1128 psia. The fuels of greatest practical interest are propane, liquid methane, and heavy hydrocarbon of the RP-1 class. The factors influencing the final fuel selection are the projected life cycle cost, propellant density, attainable specific impulse, the ability to operate preburners or gas generators without carbon fouling, and the capability of providing adequate main combustion chamber cooling at the increased operating pressure.

Presented as Paper 87-1875 at the AIAA/SAE/ASME 23rd Joint Propulsion Conference, San Diego, CA, June 29–July 2, 1987; received July 27, 1989; revision received Feb. 23, 1990.

*Research Scientist. Associate Fellow AIAA.

Previous hydrocarbon (RP-1) fueled booster engines, such as the H-1 and F-1, depended heavily on the presence of a layer of highly insulative carbon soot that deposited on the combustion chamber wall as a result of incomplete combustion of the fuel. The soot reduced the heat flux as much as 50% and thus made regenerative cooling practical with relatively low coolant pressure loss.

The combustion efficiency of some of these older engines left much to be desired (F-1 ~ 94%) as great compromises in injector element selections were known to have been made in order to achieve stable combustion. This derating in combustion efficiency also provided the wall carbon deposition necessary to enable chamber cooling. La Botz[1] and Hernandez[2] conducted combustion chamber heat transfer research programs employing LOX/RP-1 propellants in high-performing combustion devices, operated without producing a protective carbon layer on the chamber wall. Under these conditions, both experimental projects reported throat heat-flux values 50% higher than would be predicted for clean, soot-free wall using generally accepted industry standard analytical techniques.

The required reduction in operating costs for the next-generation propulsion will dictate greater propellant utilization efficiency (I_{sp}), which can only be attained by a higher operating pressure and more efficient combustion devices that generate little or no soot. The desire to also have a low-maintenance, reusable vehicle makes the cooling issue even more critical.

In order to complete the propellant selection and design optimization studies, it is essential to further define the relationship between combustion efficiency, injector design, and the chamber heat transfer characteristics.

This research provides a data base that can be useful in isolating the effect of carbon deposition and combustion efficiency on the chamber heat-flux profiles.

Approach

Two hydrocarbon-based fuels (propane and ethanol) were hot-fire tested in a water-cooled calorimeter thrust chamber. The influence of injector design was evaluated by using two different injector element designs for one of the fuels. In addition, fuel in varying amounts was uniformly sprayed around the outer periphery of the core flow to provide data relating to changes in axial heat transfer profiles and engine performance.

The peripheral fuel flow, core mixture ratio, and chamber pressure were systematically varied for each injector to establish the influence of injection momentum ratio and combustion chemistry on the resulting axial heat transfer profiles.

The test procedure involved starting each long-duration (30–60 s) test by operating the core injector at a selected pro-

pellant *O/F* and an additional specified amount of fuel injected around the periphery of the chamber. The peripheral fuel flow was terminated after steady-state thermal conditions were reached. The engine firing continued until a new thermal and performance equilibrium state was attained. Long-duration tests starting without the secondary fuel were also conducted for comparison purposes.

The water-cooled calorimeter combustion chamber shown in Fig. 1 provided nine circumferential flow segments from which heat flux vs time could be measured. The flow and instrumentation schematic from which performance and heat transfer rates were computed is provided in Fig. 2. Figures 3 and 4 show the injector patterns and essential orifice features.

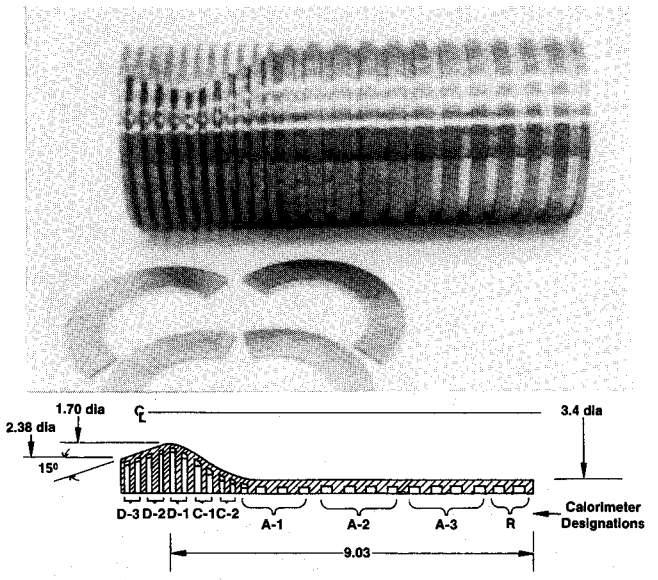

Fig. 1 Water-cooled calorimeter chamber.

The electrical discharge machine (EDM) oxygen/fuel/oxygen (OFO) triplet element produced a hydraulically atomized (momentum exchange between impacting liquid jets) spray fan. This is shown in Figs. 3 and 5. Each preatomized triplet (PAT) element consists of two oxidizer splash plate orifices and a single fuel, hollow cone swirler. The flow streams produced by the PAT are shown in Figs. 4 and 6. In this design the fuel and oxidizer are atomized prior to contact.

The separately manifolded peripheral fuel spray injector is shown in Fig. 7. The peripheral fuel spray is developed by impinging 36 fuel jets on the outer periphery of the injector through the resonator cavity, as shown in Fig. 8.

Typical heat transfer vs time data computed from the water flow rate and temperature rise measurements for each of the nine calorimeter segments are listed in Tables 1 and 2 and shown in Figs. 9, 10, and 11, respectively, for the propane/EDM, ethanol/EDM, and ethanol/PAT, fuel/injector, combinations. Figures 9a and 9b compare heat flux vs time with 14 and 9% peripheral propane injection at the start of the test. The rise in heat flux at 63 s shown in Fig. 9a corresponds to the termination of the peripheral fuel film flow. The reduction of heat flux with time in Fig. 9b is attributed to the carbon soot buildup even when no fuel film cooling is employed. The heat flux vs time data for ethanol (Figs. 11 and 12) indicate no heat-flux decrease due to sooting. Terminating the 7.2% ethanol fuel film cooling at 25 s has no significant effect on the midchamber and throat heat flux. A flux increase is observed in the resonator cavity and immediately downstream of the injector. A comparison of throat station flux in Figs. 10 and 11 reveals no significant heat-flux reductions even when the fuel coolant flow is increased to 16.8%. Termination of the coolant at 26 s in Fig. 11 actually reduces the heat flux somewhat. The reason for this is discussed later.

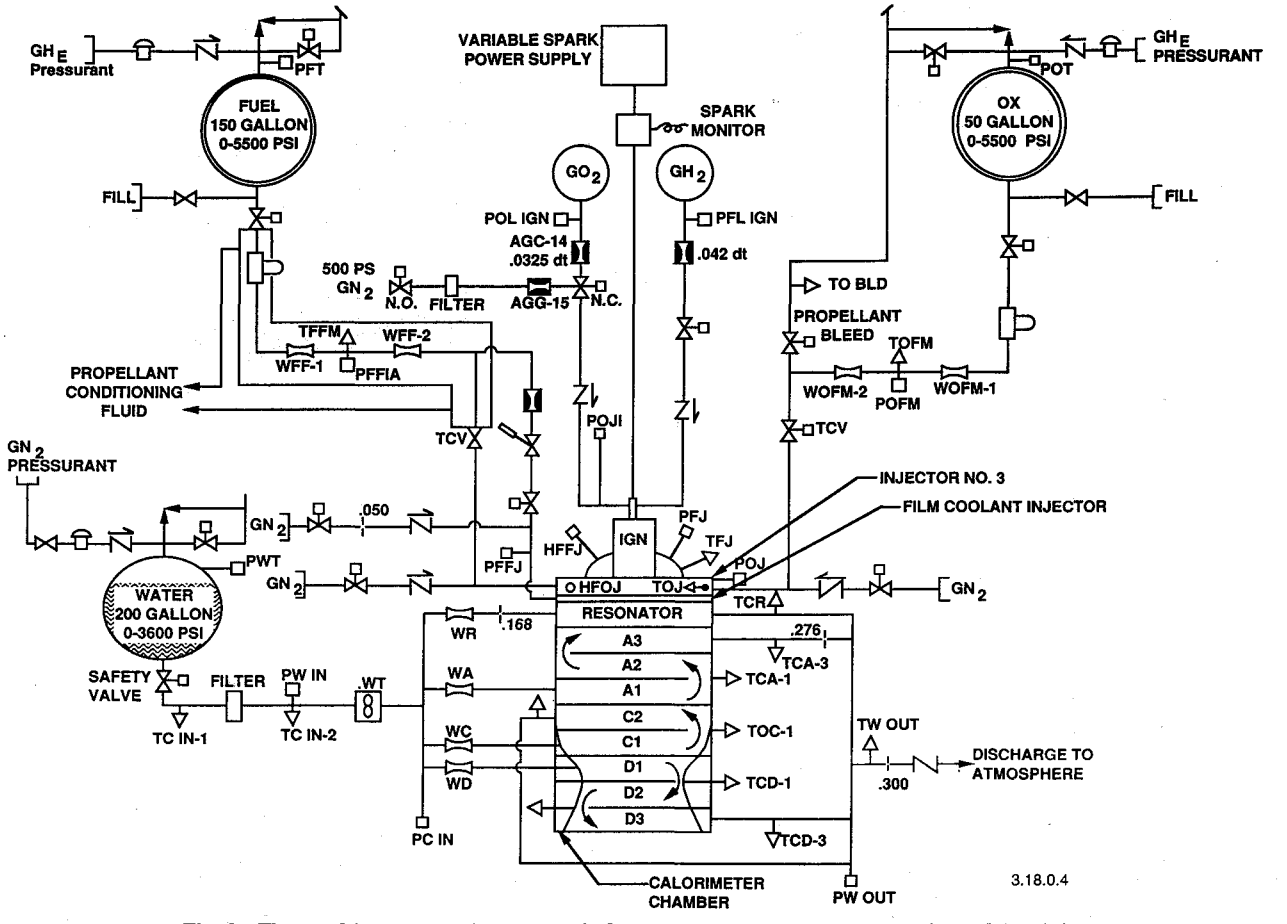

Fig. 2 Flow and instrumentation schematic for water-cooled chamber with peripheral fuel injector.

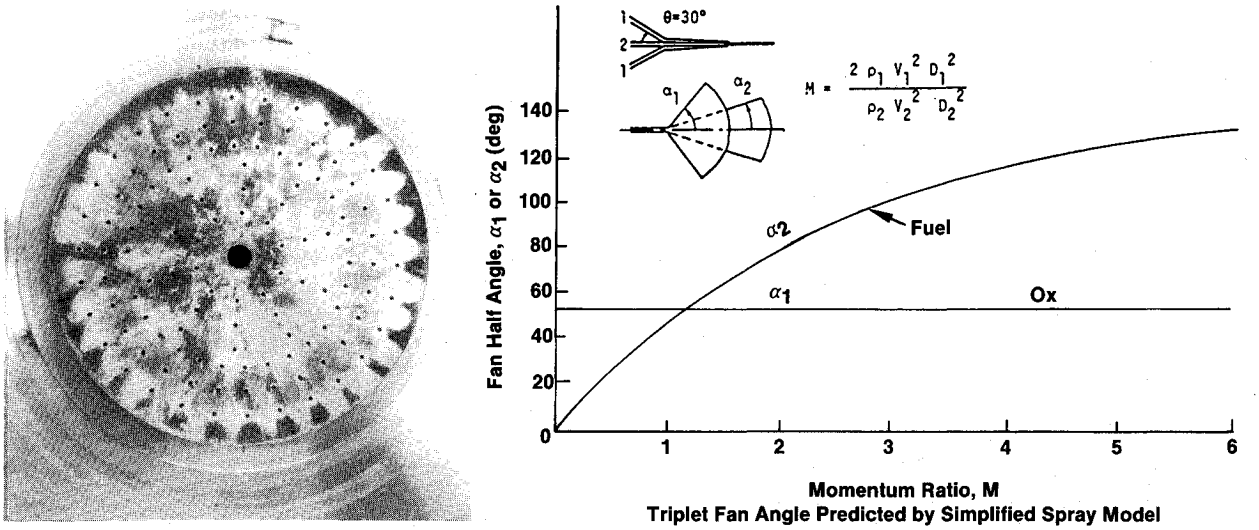

Fig. 3 Forty-element EDM-OFO triplet injector.

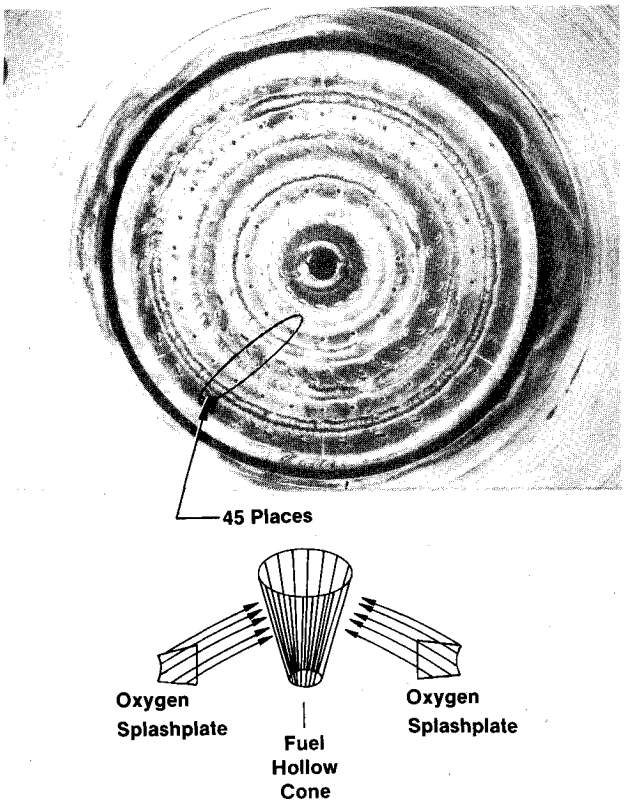

Fig. 4 Forty-five-element OFO PAT after test.

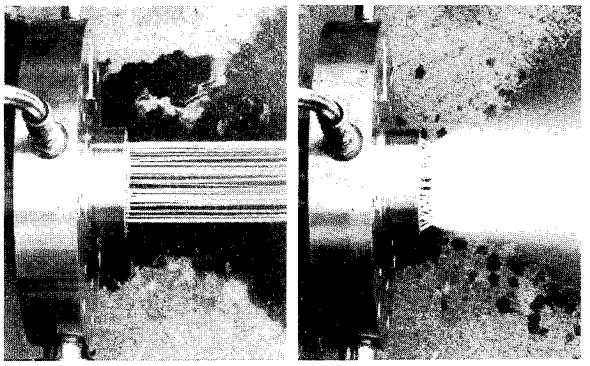

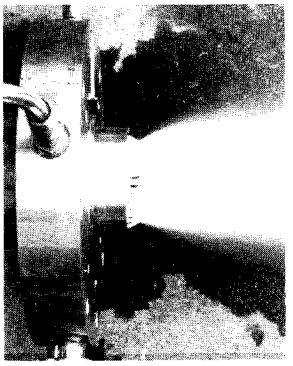

Fig. 5 EDM-OFO triplet injector cold flow.

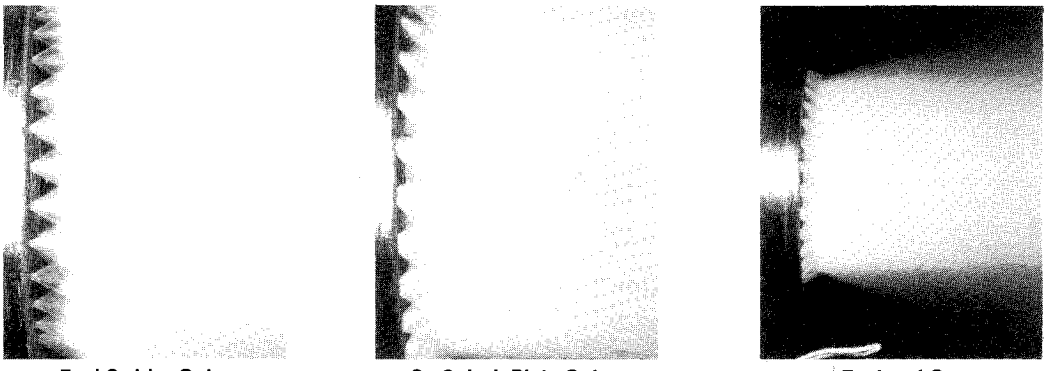

Fig. 6 Preatomized triplet (PAT) injector cold flow.

Discussion of Test Results

Performance

Both injectors resulted in energy release efficiencies greater than 99% at the design *O/F* as noted in Fig. 12. The difference in hydrogen-to-carbon ratios in the two fuels, propane (C_3H_8) and ethanol (C_2H_5OH), resulted in different optimum *O/F*. The figure displays the effect of changes in the relative propellant flow ratios on the combined vaporization and mixing efficiency (ERE). Changing the total flow rate (i.e., higher or lower chamber pressure) at a fixed momentum ratio had only second-order effects on ERE. The effect of changes in the propellant injection momentum ratio on the thermal profiles is discussed later.

Table 3 shows the effect of peripheral fuel addition on measured specific impulse. A significant loss in specific impulse is noted when 14% peripheral propane is added. In contrast, only a minor loss is noted when the same percentage of ethanol is added using the same injector.

When the injector is changed to the PAT, a significant increase in performance is noted when peripheral ethanol is added. The periphery of this injector core operates oxygen

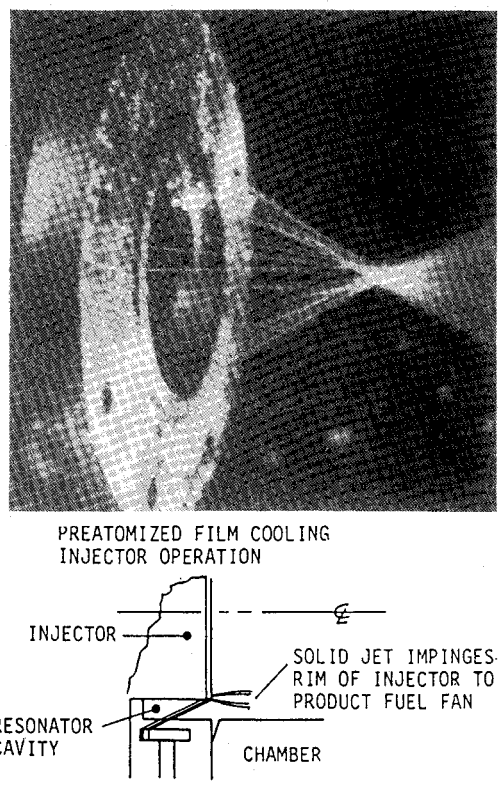

Fig. 7 Injector used for fuel enrichment of the boundary-layer flow.

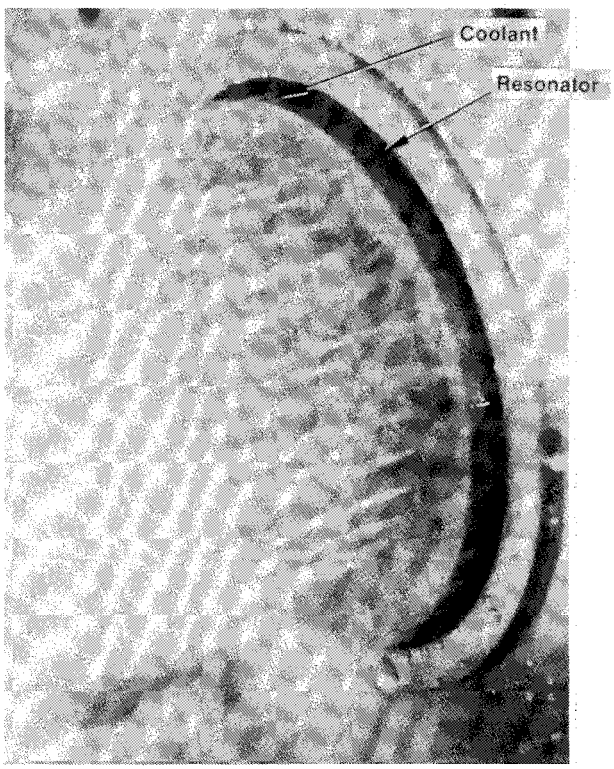

Fig. 8 OFO triplet injector and peripheral fuel flow only.

Table 1 Test conditions and thermal parameters for LOX/propane and OFO triplet injector

Axial distance, in.:					0.5	2	4	6	7.5	8.5	9	9.5	10				
						Heat flux, Btu/s-in.^{2}											
Test run	Start time	Eng. *MR*	P_c	W_t[a]	QR	QA-3	QA-2	QA-1	QC-2	QC-1	QD-1	QD-2	QD-3	Total *Q*, Btu/s	Core *MR*	%FFC	WFC
146	2.0	2.26	300	3.89901	1.09	3.15	3.06	2.43	2.29	3.16	4.18	2.72	1.96	258		14.6	0.174257
	10	2.25	304	3.92201	1.27	2.81	2.13	1.54	1.33	2.15	4.11	2.54	2.01	215	2.63	14.4	0.173763
	20	2.24	306	3.92815	1.18	2.06	1.20	1.26	1.28	2.52	4.03	1.67	1.57	189	2.61	14.2	0.172848
	FS-2	2.55	306	3.80825	2.81	2.81	2.30	3.17	2.73	5.02	6.92	3.71	2.56	337		0	0
147	2.0	1.59	306	2.64876	0.71	2.52	2.47	2.28	2.20	2.84	4.14	2.52	1.82	215		14.6	0.244062
	10	1.54	311	2.60488	0.79	2.34	1.79	1.52	1.48	1.90	3.53	2.12	1.85	186	1.8[b]	14.6	0.246013
	20	1.53	314	2.60240	0.87	2.09	1.44	1.26	1.61	1.79	3.15	1.95	1.79	164	1.8[b]	14.6	0.247895
	FS-2	1.78	312	4.11402	3.13	4.82	4.90	4.45	3.72	5.34	8.13	5.21	3.52	455		0	0
148	2.0	3.62	304	4.06126	0.77	2.51	2.88	2.50	2.27	3.14	4.99	3.77	2.67	244		14.2	0.126656
	10	3.75	302	4.05066	0.82	1.93	1.78	1.65	1.82	2.85	4.88	4.25	3.34	201	4.37	14.1	0.120153
	20	3.63	309	4.06661	0.71	1.63	0.98	1.45	1.70	2.75	4.15	3.64	3.14	172	4.23	14.0	0.123237
	FS-2	4.04	306	4.00331	1.40	1.95	1.69	2.69	3.29	5.45	9.32	7.43	5.39	282		0	0
149	2.0	2.41	302	3.92563	1.36	3.44	2.99	2.86	2.90	4.07	5.87	3.89	2.69	287		8.4	0.099361
	10	2.50	305	3.86073	1.42	3.28	2.57	2.30	2.23	3.13	4.93	4.00	2.66	269	2.73	8.3	0.092214
	20	2.47	309	3.86248	1.52	2.82	2.13	2.21	2.01	3.02	4.57	3.35	2.70	250	2.70	8.3	0.092403
	FS-2	2.61	308	3.79591	2.48	3.38	3.17	3.28	2.87	4.41	6.09	4.89	3.91	339		0	0
151	2.0	1.94	203	2.78965	0.54	1.94	2.02	1.99	1.89	2.60	3.44	2.15	1.59	177		14.7	0.140218
	10	2.09	203	2.70938	0.69	2.05	2.01	1.85	1.75	2.27	2.82	1.85	1.62	188	2.45	14.5	0.127426
	20	2.11	206	2.65952	0.58	1.94	1.84	1.35	1.62	1.87	2.91	1.56	1.41	172	2.47	14.4	0.123691
	FS-2	2.39	205	2.61055	2.81	3.18	3.28	3.25	2.84	4.06	5.14	3.65	3.67	321	——	0	0
152	2.0	2.17	408	5.25099	1.24	3.68	3.00	2.62	2.06	3.20	5.65	3.47	2.41	283		15.5	0.260970
	10	2.15	413	5.25659	1.33	3.02	1.93	1.76	2.23	3.31	6.16	3.67	2.80	237	2.55	15.4	0.256975
	20	2.10	416	5.28544	1.14	2.72	1.55	1.72	2.54	3.85	6.01	3.57	2.40	226	2.49	15.2	0.260055
	FS-2	2.42	413	5.07460	3.15	5.10	5.07	4.36	4.15	6.93	10.36	5.85	4.26	495	——	0	0

[a]Total propellant flow rate. [b]Estimated.

Table 2 Test conditions and thermal parameters for LOX/ethanol with OFO triplet injector

Test run	Time, s	Eng. *MR*	Core *MR*	P_c, psia	$\dot{W}_T$, lbm/s	%FFC, %fuel	$\dot{W}_{FFC}$, lbm/s	%FFC, %total	$\dot{Q}_{total}$, Btu/s	Heat flux $\dot{Q}/A$, Btu/in.^{2}-s								
										0.5	2	4	6	7.5	8.5	9	9.5	10
										R	A-3	A-2	A-1	C-2	C-1	D-1	D-2	D-3
153	2.0	1.54	1.79	291	3.95	14.2	0.222	5.62	329.5	1.05	2.53	3.97	3.77	3.44	5.51	10.38	6.30	4.28
155	2.0	1.46	1.71	291	3.97	14.2	0.228		334.4	1.09	2.34	3.97	3.85	3.35	5.64	10.5	6.39	4.24
	5.0	1.46	1.71	294	3.97	14.2	0.229	5.76	371.3	1.10	2.54	4.14	3.82	3.56	6.06	11.3	7.00	4.84
									380	1.1	2.7	4.3	3.95	3.95	6.35	11.65	7.3	5.10
156	2.0	1.20	1.41	276	3.91	14.3	0.252		282.5	0.92	1.75	3.17	3.43	3.15	5.03	9.52	5.64	3.79
	5.0	1.19	1.39	376	3.90	14.4	0.256		320.0	1.02	1.83	3.32	3.49	3.26	5.44	10.22	6.04	4.26
	10.0	1.18	1.38	277	3.93	14.4	0.259		325.4	1.06	1.84	3.32	3.39	3.32	5.51	10.42	6.21	4.39
	20.0	1.18	1.38	279	3.92	14.3	0.257	6.55	328.9	0.90	1.85	3.35	3.37	3.36	5.64	10.58	6.26	4.48
	FS-2/30	1.36	1.36	272	3.79	0	0		388.2	3.54	3.44	3.21	3.35	3.55	6.08	11.30	7.33	5.30
157	2.0	1.21	1.41	279	3.94	14.3	0.255											
	5.0	1.20	1.40	280	3.96	14.4	0.259											
	20.0	1.18	1.38	283	3.97	14.4	0.262	6.60	338.3	0.98	1.87	3.44	3.38	3.39	6.31	11.21	6.21	4.43
	FS-2/30	1.37	1.37	276	3.85	0	0		395.0	3.54	3.47	3.28	3.26	3.50	6.23	11.67	7.45	5.20
158	2.0	1.74	1.88	288	3.84	7.2	0.101											
	5.0	1.72	1.86	289	3.86	7.6	0.108											
	20.0	1.69	1.83	293	3.88	7.8	0.113	2.90	459.6	1.31	3.46	4.49	4.36	4.16	7.31	14.58	8.33	5.81
	FS-2/30	1.82	1.82	289	3.84	0	0		483.9	3.27	4.48	4.36	4.18	4.16	7.18	14.43	8.54	5.92
159	2.0	2.13	2.48	291	3.92	13.9	0.174											
	5.0	2.13	2.47	292	3.93	14.0	0.175											
	20.0	2.09	2.44	296	3.95	14.0	0.178	4.52	409.3	1.28	3.00	4.04	3.70	3.54	7.06	13.91	7.25	5.26
	FS-2/30	2.35	2.35	292	3.88	0	0		504.1	2.80	4.45	4.80	4.37	4.20	7.43	15.68	8.95	6.02
160	2.0	1.67	1.95	384	5.11	14.5	0.280	5.44	441.4	1.21	3.80	5.09	4.44	4.11	8.55	15.80	7.64	4.94
	5.0	1.66	1.94	388	5.13	14.6	0.282		505.5	1.38	4.03	5.25	4.66	4.37	9.32	16.91	8.49	5.75
	20.0	1.65	1.93	391	5.16	14.6	0.283	5.51	528.5	1.55	4.05	5.36	4.70	4.49	9.65	17.5	8.80	6.04

Run	P_c	*MR*	W_T	Section	Heat flux	C_{gf}	C_{gs}
156	272	1.36	3.79	R	3.54	0.0241	0.0181
No film cooling				A-3	3.44	0.0234	0.0176
				A-2	3.21	0.0219	0.0164
				A-1	3.35	0.0228	0.0171
				C-2	3.55	0.0193	0.0145
				C-1	6.08	0.0206	0.0155
				D-1	11.30	0.0245	0.0184
				D-2	7.33	0.0194	0.0145
				D-3	5.30	0.0204	0.0153
157	276	1.37	3.85	R	3.54	0.0238	0.0179
No film cooling				A-3	3.47	0.0233	0.0175
				A-2	3.28	0.0221	0.0166
				A-1	3.26	0.0219	0.0164
				C-2	3.50	0.0188	0.0141
				C-1	6.23	0.0208	0.0156
				D-1	11.67	0.0249	0.0187
				D-2	7.45	0.0195	0.0146
				D-3	5.20	0.0198	0.0148
158	289	1.82	3.84	R	3.27	0.0220	0.0153
No film cooling				A-3	4.48	0.0302	0.0210
				A-2	4.36	0.0294	0.0205
				A-1	4.18	0.0282	0.0197
				C-2	4.16	0.0224	0.0156
				C-1	7.18	0.0240	0.0167
				D-1	14.43	0.0305	0.0212
				D-2	8.54	0.0215	0.0150
				D-3	5.92	0.0207	0.0144
159	292	2.35	3.88	R	2.80	0.0205	0.0140
No film cooling				A-3	4.45	0.0326	0.0222
				A-2	4.80	0.0352	0.0240
				A-1	4.37	0.0320	0.0218
				C-2	4.20	0.0246	0.0168
				C-1	7.43	0.0270	0.0184
				D-1	15.68	0.0358	0.0244
				D-2	8.95	0.0243	0.0165
				D-3	6.02	0.0227	0.0154
		1.69 Engine					
158	293	1.83 Core	3.88	R	1.31	0.0088	0.0063
7.8% Fuel film cooling				A-3	3.46	0.0231	0.0164
				A-2	4.49	0.0300	0.0213
				A-1	4.36	0.0292	0.0208
				C-2	4.16	0.0222	0.0158
				C-1	7.31	0.0242	0.0172
				D-1	14.58	0.0303	0.0215
				D-2	8.33	0.0206	0.0146
				D-3	5.81	0.0200	0.0142

Local diameter vs station: R = A-1, A-2, A-3 = 3.40-in. diam.; C_2 = 2.998 in., C_1 = 2.294 in.; D_1 = 1.740 in., D_2 = 1.878 in., D_3 = 2.206 in.

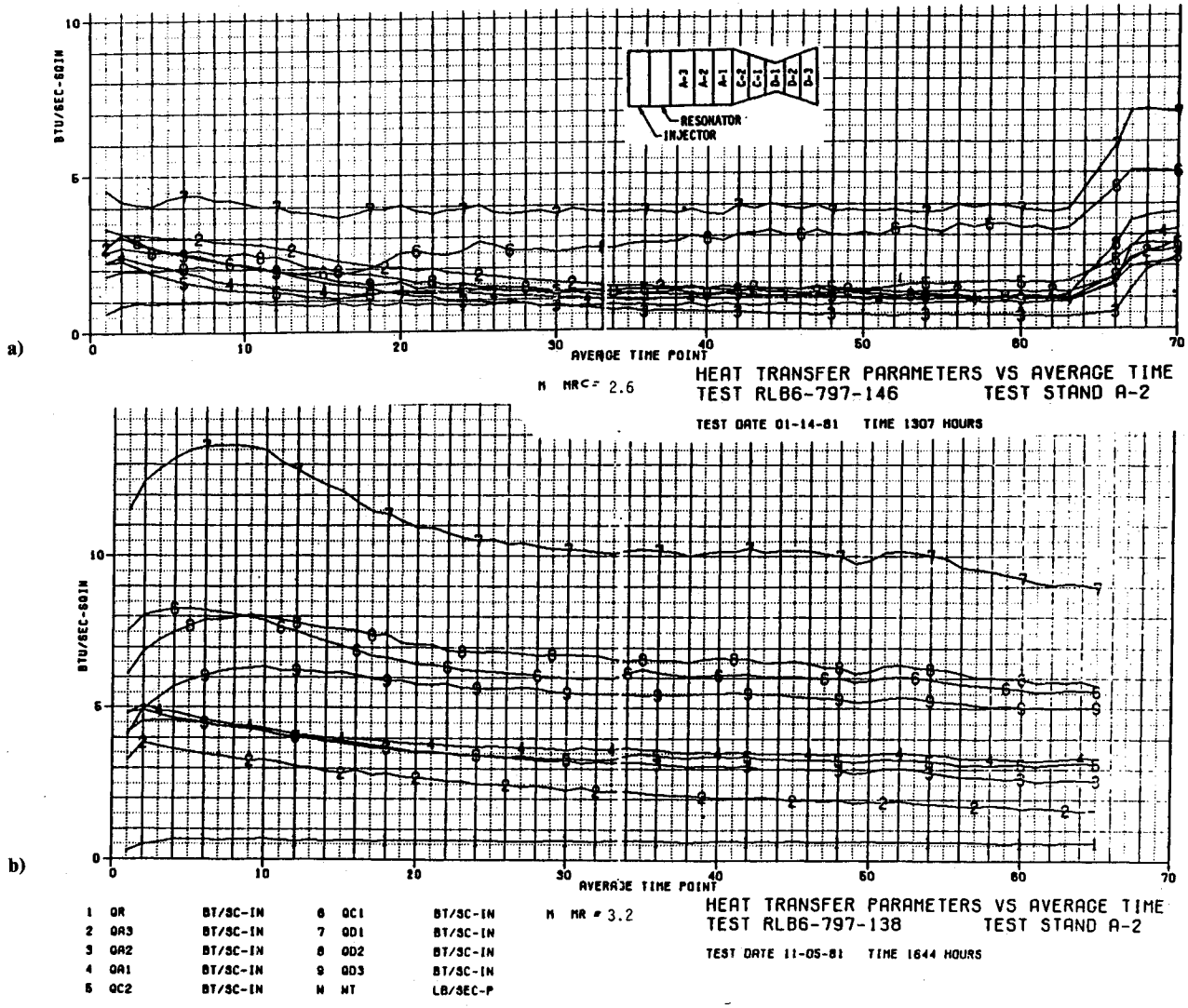

Fig. 9 Heat flux vs time, LOX propane, EDM OFO injector: a) 14% peripheral fuel, 0–63 s, 0% peripheral fuel, 63–70 s, $O/F = 2.6$; b) 0% peripheral fuel, 0–65 s, $O/F = 3.2$.

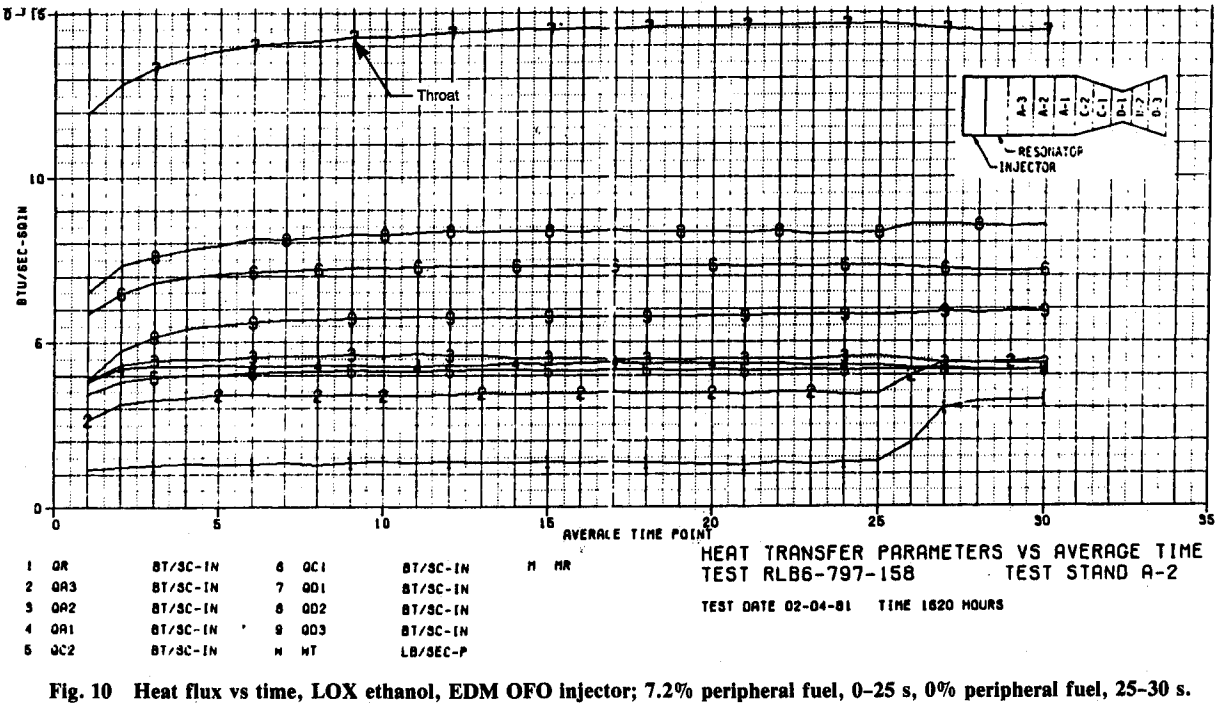

Fig. 10 Heat flux vs time, LOX ethanol, EDM OFO injector; 7.2% peripheral fuel, 0–25 s, 0% peripheral fuel, 25–30 s.

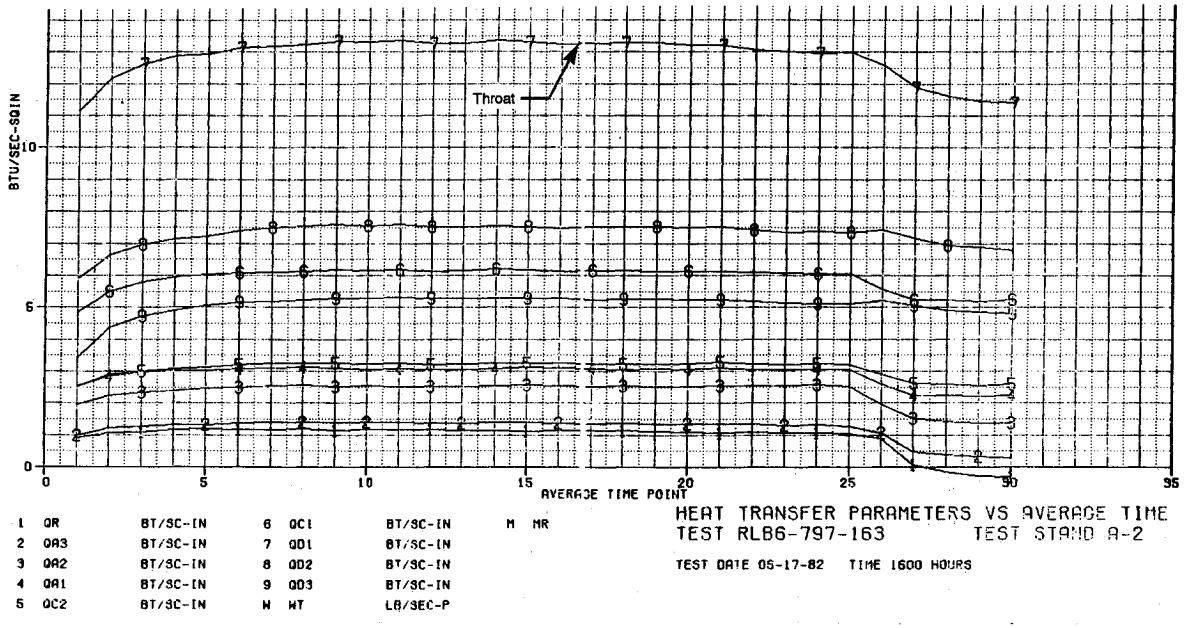

Fig. 11 Heat flux vs time, LOX ethanol, PAT platelet injector; 16.8% peripheral fuel, 0–16 s, 0% peripheral fuel, 26–30 s.

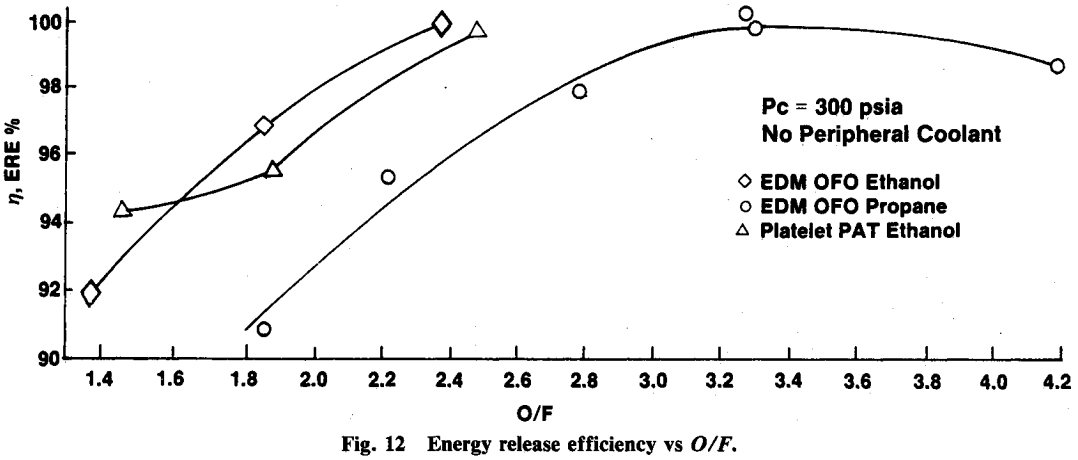

Fig. 12 Energy release efficiency vs *O/F*.

rich, and the addition of fuel increases both performance and heat flux.

Visual Results

The fuels employed in testing provided significantly different sooting characteristics. Propane burns with a brilliant yellow-white flame, as shown in Fig. 13a, and produces significant sooting. The ethanol, in contrast, provides a clear blue exhaust, as shown in Fig. 13b, and produces no carbon soot.

Post-test inspection of injector and chamber following the propane testing revealed that the heaviest face and wall sooting occurred during the high *O/F* tests. These visual observations agreed with the thermal data and were subsequently correlated with the injection momentum ratio for the OFO triplet, as discussed in detail by Schoenman.[3] In summary, and as illustrated in Fig. 3, a high oxygen/fuel momentum ratio for the OFO element imparts a large transverse flow component to the impacted center fuel jet. The increased transverse flow places more fuel on the wall at the chamber head end.

The resonator cavities were noted to be filling with hard carbon deposits in early tests in which no fuel was injected around the periphery of the injector. This carbon buildup can reduce the resonator effectiveness and change the resonator cavity tuning. This is cause for concern for a reusable engine, since cleaning the cavities of carbon between flights will increase operational costs.

The ethanol produced no soot on the injector face, chamber wall, or in the resonator cavity at any *O/F*.

Thermal Results

A comparison of the theoretical combustion temperatures and heat transfer rates is given in Fig. 14. The analysis predicts that the heat flux for the two fuels should be within 10% with propane being the hotter of the two.

The experimental heat flux for the two fuels and the two injector patterns is shown in Figs. 15–18. Without peripheral fuel injection the LOX/propane (*O/F* = 3.2 at 300 psia) yields a maximum throat heat flux of 11 Btu/in.-s early in the test. This decays to 8 Btu/in.^{2}-s after the soot buildup stabilizes. Data shown later demonstrated that as little as 8.5% peripheral propane addition will decrease the throat heat flux to 4 Btu/s-in. Using the same injector, chamber pressure, and appropriate *O/F* with ethanol produces a maximum heat flux of 16, which remains stable throughout the test. The PAT injector yields maximum heat flux values of 13.5 and 15 at *O/F* of 1.9 and 2.4 with ethanol. These also remain constant throughout the test. The addition of up to 16% of the ethanol in peripheral flow has no significant impact on the throat heat flux, as noted by curve 7 in Figs. 10 and 11 and Fig. 16.

Figure 17 shows the axial heat flux profiles, without peripheral injection, for the two injectors tested with ethanol. The low head-end flux with the PAT is caused by excess LOX on the chamber wall. This is confirmed by the data in Fig. 18,

Table 3 Effect of film fuel coolant on I_{sp}, ϵ = 4:1

	FFC[a]		
Injector/fuel	0%	8%	14%
EDM/propane	257.0	254.0	246.0
EDM/ethanol	237.8	—	236.9
PAT/ethanol	233.7	—	241.7

[a]FFC, fuel film cooling.

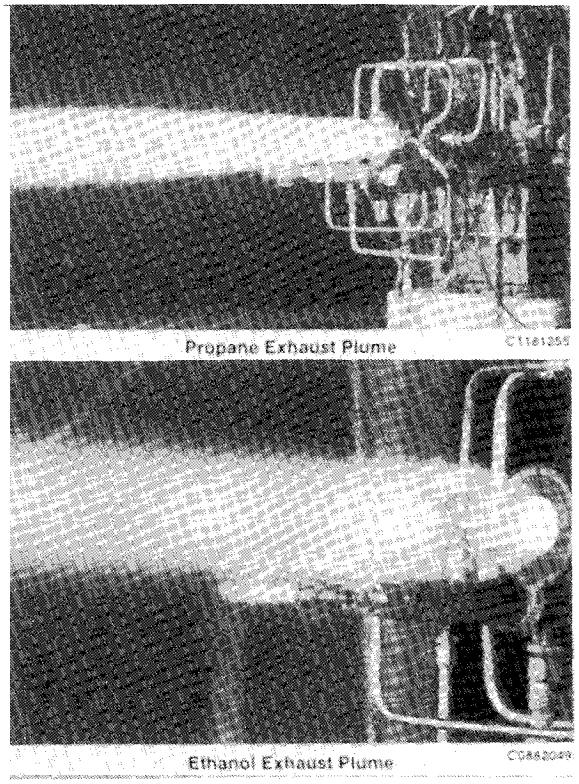

Fig. 13 Comparison of exhaust plumes for propane and ethanol.

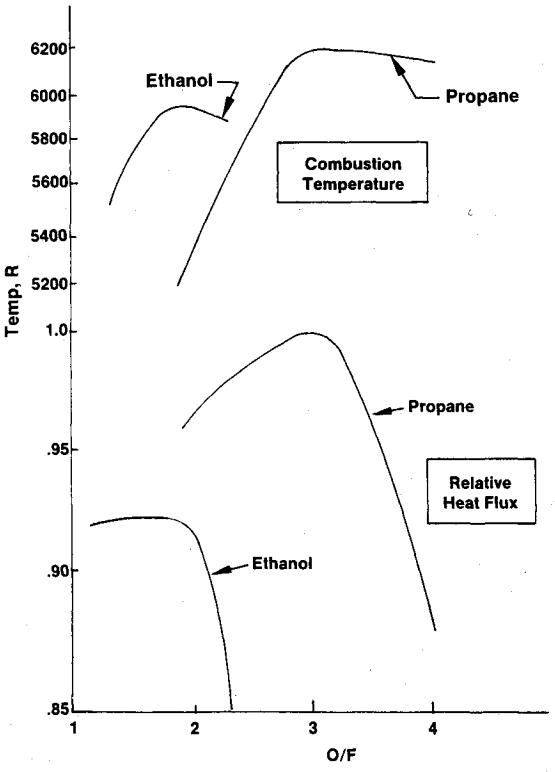

Fig. 14 Comparison of combustion temperature and relative theoretical heat flux vs O/F for LOX/propane and LOX/ethanol.

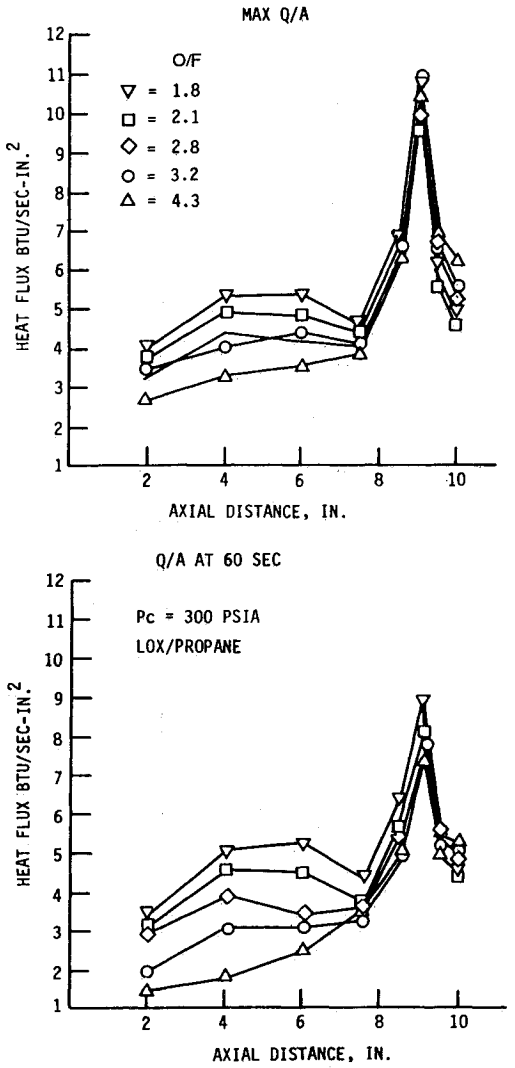

Fig. 15 Effect of mixture ratio O/F on LOX propane heat-flux profiles at the time of maximum flux and at 60 s.

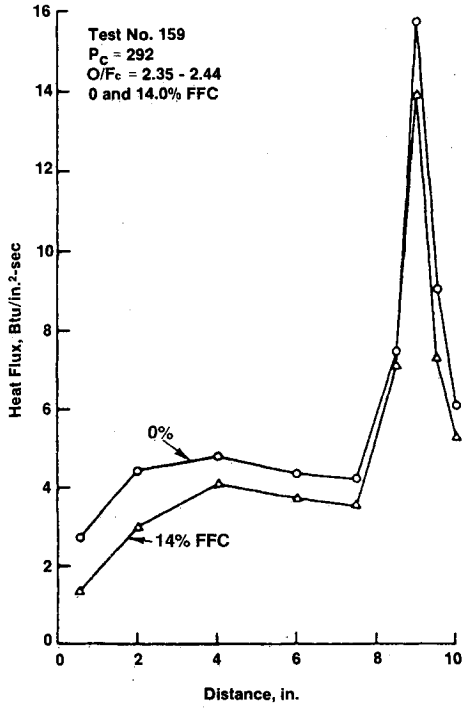

Fig. 16 Effect of peripheral ethanol addition on axial heat-flux profile, EDM-OFO, $P_c \approx 300$.

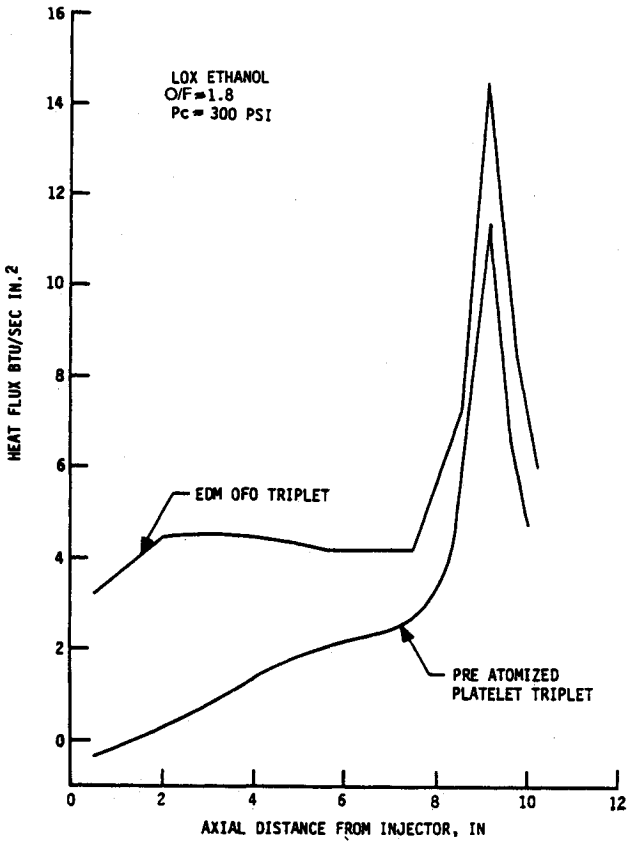

Fig. 17 Comparison of EDM and platelet injector heat-flux profiles without peripheral fuel injection.

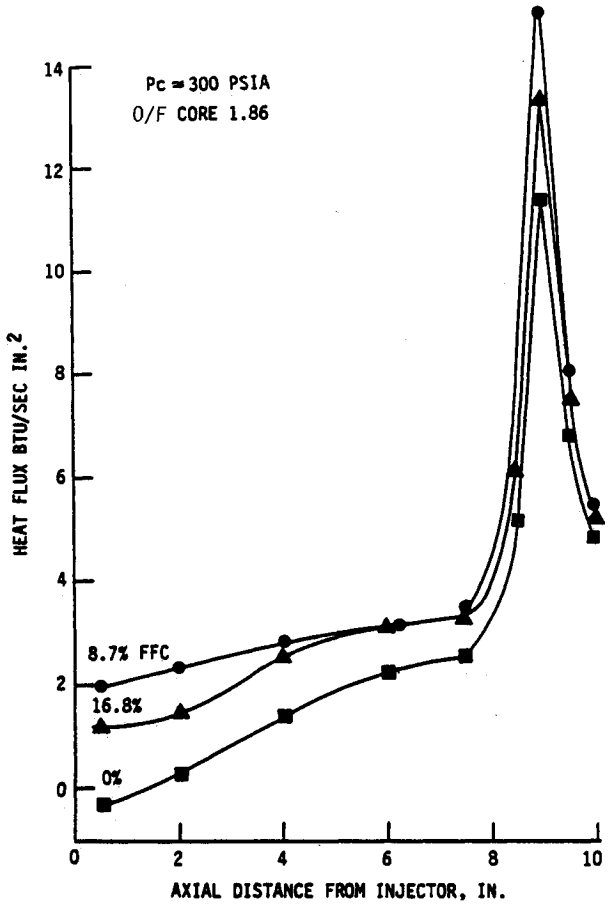

Fig. 18 Heat flux vs distance for platelet PAT injector with LOX/ethanol propellants, peripheral fuel injection 0-16.8%.

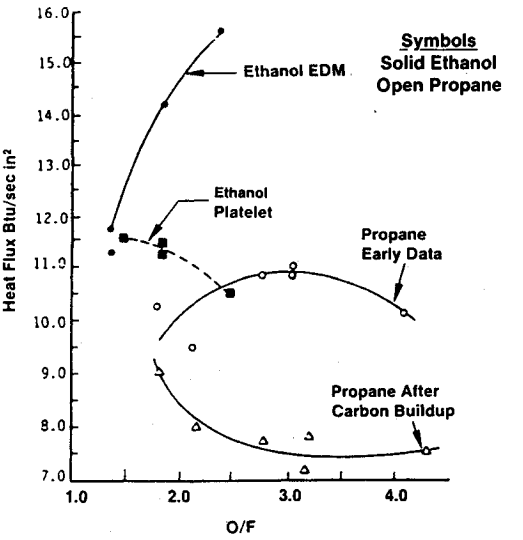

Fig. 19 Maximum and steady-state throat heat-flux profiles vs *O/F* for two injectors and two fuels.

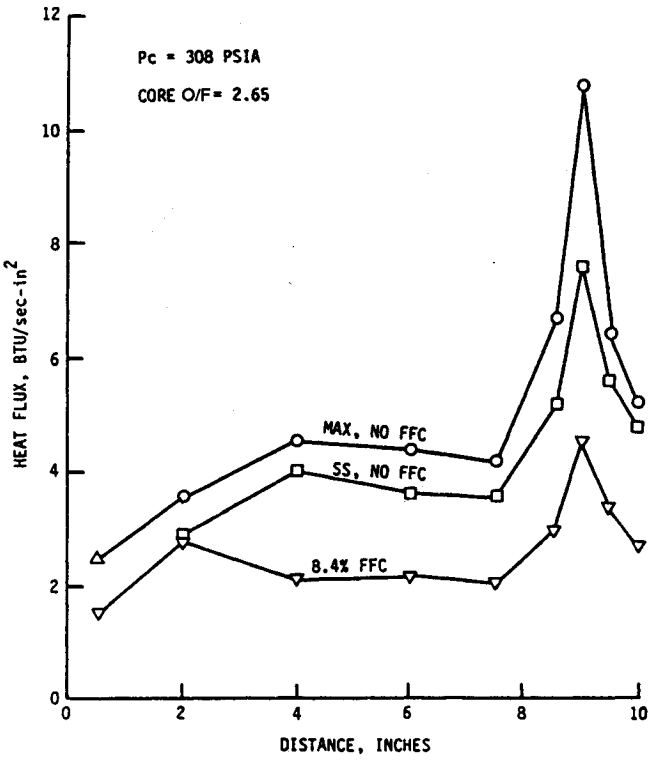

Fig. 20 Effect of peripheral propane injection and time on axial heat-flux profiles, *O/F* = 2.6.

which show increased head-end and throat heat flux when fuel is injected at the periphery. At 8.7% fuel injection the throat flux reaches 14 Btu/in.-s, which is identical to the EDM OFO design. Figure 19 shows the injector and *O/F* effects on the throat heat flux. The ethanol tested with the EDM OFO pattern produces a significant increase in throat heat flux as the *O/F* ratio is increased and reaches a value two times greater than that with propane when an equilibrium carbon soot layer is attained, or four times greater when the carbon soot layer is enhanced by added peripheral fuel.

The throat heat flux for propane with the OFO pattern shows a significant wall soot buildup as the *O/F* is increased.

Figures 20 and 21 provide a comparison of the axial heat-flux profiles and the effect of propane injection around the periphery. The profiles in the two figures straddle the *O/F* that

produces optimum performance. The addition of propane around the injector periphery is noted to significantly reduce the heat flux along the entire length of the chamber, with throat flux reductions approaching 60%.

One of the most significant aspects of this test program was the high throat heat flux experienced with ethanol. As shown in Figs. 22 and 23, the throat flux was more than 50% higher than would be predicted using industry standard predictive methods that have been proven to be valid for O_2/H_2 and N_2O_4/MMH propellants. Standard heat-flux prediction methods include throat flow acceleration effects, which depress the turbulence level in the boundary layer, and thus the throat C_g [defined by Eq. (1)], as illustrated by the dashed curve of Fig. 22:

$$C_{g_f} = \frac{(Q/A)D^{1.8}}{(\dot{w}_t)^{0.8}(T_r - T_{w_g})(T_e/T_f)^{0.8}(4/\pi)^{0.8}C_{p_f}Pr_f^{-0.6}} \quad (1)$$

Von Glahn[4] and Back et al.[5,6] also reported this effect. In contrast, the rapid drop in pressure in the throat region ap-

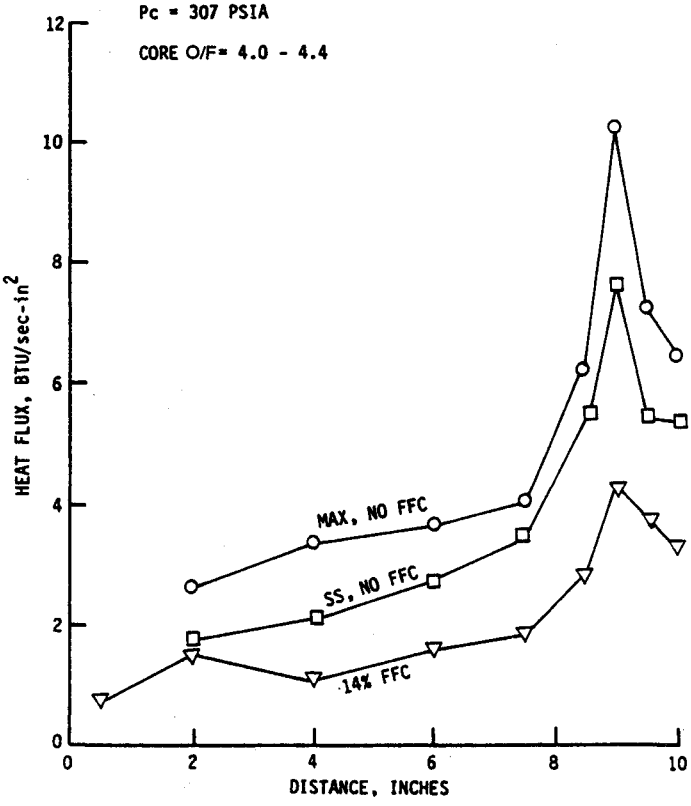

Fig. 21 Effect of peripheral propane injection and time on axial heat-flux profiles, O/F = 4.

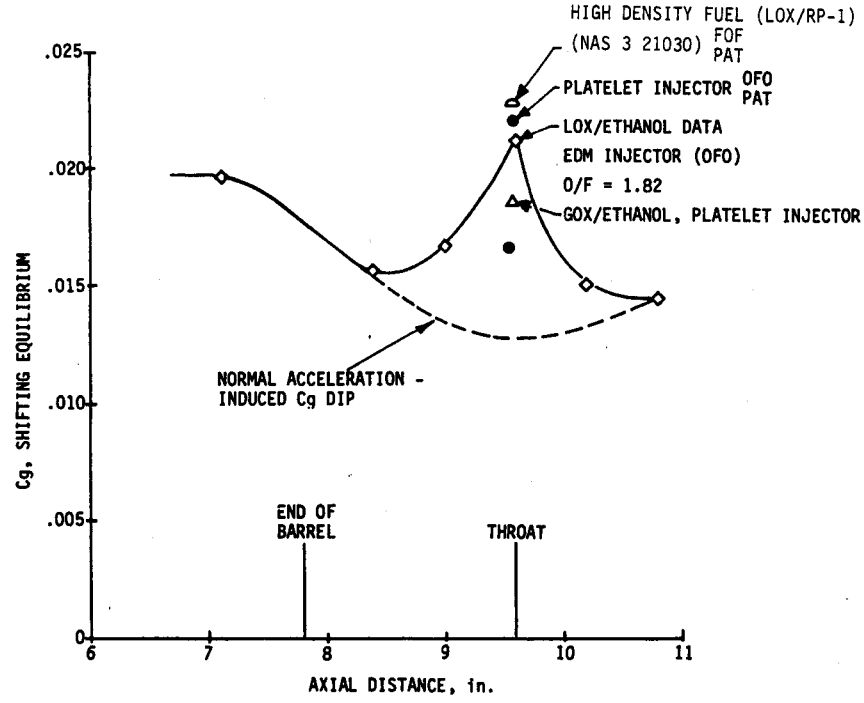

Fig. 22 Comparison of experimental heat-flux profiles with predicted fluxes using contemporary methods.

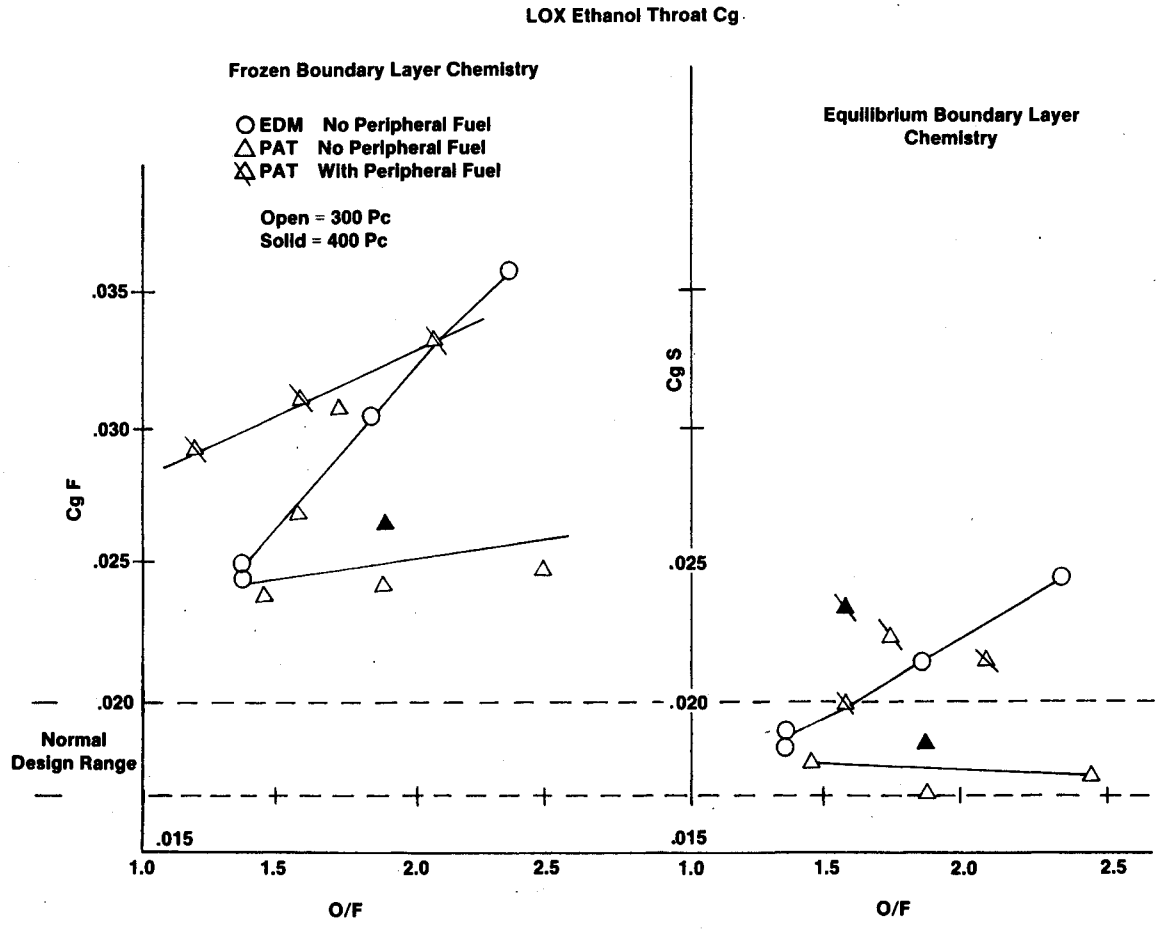

Fig. 23 LOX/ethanol throat C_g.

pears to be triggering a heat-transfer-enhancing mechanism that has not been observed for the O_2/H_2 and N_2O_4/MMH propellant combinations. There are no industry standards defining heat-flux computations for nonequilibrium combustion in regions of high-pressure gradients and highly cooled walls. However, an enthalpy-based driving force ΔH is sometimes employed. The variables C_{g_f} and C_{g_s} can be employed to compare the temperature- and enthalphy-based analytical procedures for heat-flux predictions. The higher heat flux can be partially explained by using a model that assumes equilibrium chemical reaction in the boundary, as illustrated by C_g in Fig. 23.

Conclusions

The present data demonstrate that the injection of small amounts of carbon soot-forming fuels such as propane along the wall can reduce the heat flux by as much as 60%. The conditions that produce sooting are sensitive to injector element type and the optimization parameters. The heat-flux masking soot builds rapidly during each test and precludes definition of a truly clean wall heat flux with propane as a fuel.

The experimental LOX/ethanol data confirm the higher-than-predicted throat heat-flux values reported in Refs. 1 and 2, when oxygen and hydrocarbon fuels are combusted in a rocket nozzle without the presence of wall sooting. No valid explanation has been presented in previous work.

Since higher-than-predicted heat-flux results have now been reported on three occasions, using different test apparatus, it is optimistic to assume that an advanced, high-performance, reusable, hydrocarbon fuel booster engine will be immune to this unpredictable phenomena or that the problem can be buried in soot. The choice of methane as the fuel or the proposed addition of H_2 as a coolant and second fuel can be expected to minimize the wall soot buildup. Improvements in hydrocarbon-fueled injector design and combustion efficiency can also be expected to reduce the sooting and potentially exposing the wall to heat-flux values considerably higher than anticipated.

References

[1]La Botz, R. J., "High-Density Fuel Combustion and Cooling Investigation," NASA CR-165177, Sept. 1980.

[2]Hernandez, R., "Carbon Deposition Model for O/Hydrocarbon Combustion," NAS 8-34715, Final Rept., 1987.

[3]Schoenman, L., "Combustion Performance and Heat Transfer Characterization of LOX/Hydrocarbon-Type Propellants," Vol. II, NAS 9-15958, Final Rept., Sept. 1983.

[4]Von Glahn, W. H., "Correlation of Gas-Side Heat Transfer for Axisymmetric Rocket Engine Nozzles," NASA TM-X1748, Feb. 1969.

[5]Back, L. H., Massier, P. F., and Cuffel, R. F., "Some Observations on Reduction of Turbulent Boundary-Layer Heat Transfer in Nozzles," *AIAA Journal*, Vol. 4, Dec. 1966, pp. 2226–2229.

[6]Back, L. H., Massier, P. F., and Cuffel, R. F., "Flow Phenomena and Convective Heat Transfer in a Conical Supersonic Nozzle," *Journal of Spacecraft and Rockets*, Vol. 4, No. 8, Aug. 1967, pp. 1040–1047.